Journal of ELECTRONIC MATERIALS, Vol. 44, No. 2, 2015
DOI: 10.1007/s11664-014-3541-3

Structural Properties of Ultrasonically Sprayed Al-Doped ZnO (AZO) Thin Films: Effect of ZnO Buffer Layer on AZO

B.J. BABU,[1,2] S. VELUMANI,[1,3,6,7] J. ARENAS-ALATORRE,[4] A. KASSIBA,[2] JOSE CHAVEZ,[5] HYEONSIK PARK,[3] SHAHZADA QAMAR HUSSAIN,[3] JUNSIN YI,[3,8] and R. ASOMOZA[1]

1.—Department of Electrical Engineering-SEES, CINVESTAV-IPN, Col San Pedro Zacatenco, C.P 07360 Mexico, D.F., Mexico. 2.—Institute of Molecules and Materials, UMR-CNRS 6283, Université du Maine, Avenue O. Messiaen, 72085 Le Mans, France. 3.—College of Information and Communication Engineering, Sungkyunkwan University, Suwon 440-746, Republic of Korea. 4.—Institute of Physics, Universidad Nacional Autónoma de México, A. P. 20-364México, D.F. 01000, Mexico. 5.—Instituto Investigaciones en Materiales-UNAM, Ciudad Universitario, Mexico, D.F., Mexico. 6.—e-mail: vels64@yahoo.com. 7.—e-mail: velu@cinvestav.mx. 8.—e-mail: yi@skku.edu

Transparent aluminium-doped ZnO (AZO)-conducting oxide films were deposited on a glass substrate, using an ultrasonic spray pyrolysis (USP) system at 475°C. We investigated the effects of the Al/Zn atomic ratios on the structural properties of the AZO films. All the deposited AZO thin films presented hexagonal wurtzite structure. As Al doping increased in the film, the preferential orientation switched from [002] to [101], and crystallite sizes varied from 31.90 nm to 34.5 nm. Field emission scanning electron microscopy showed a change in the surface morphology of the AZO films with respect to the Al/Zn ratio, and secondary ion mass spectroscopy showed that the amount of Al incorporated into the films was proportional to the concentration of the starting solution. A fast Fourier transform of the AZO film measurements confirmed the presence of (100), (102), and (200) reflections, corresponding to a wurtzite structure of the AZO thin films. The plane corresponding to AZO was simulated, and matched the experimental pattern obtained from high-resolution transmission electron microscopy. An un-doped ZnO layer was deposited onto the AZO film using USP at 400°C, and a bilayer of AZO/ZnO was annealed in vacuum for 20 min at 350°C. The resistivity of these bilayer films was lower than that of a single-layered AZO film, and it further decreased by vacuum annealing.

Key words: AZO, USP, AZO/ZnO, vacuum annealing

INTRODUCTION

Zinc oxide is an *n*-type, wide band-gap semiconductor that has many attractive features, and has been mostly investigated for use as a transparent conducting oxide (TCO) layer. The important physical properties of the material, namely the electro-optical, acoustic-optical, piezo-electrical, and luminescent properties, render the thin film of zinc oxide a suitable material for a wide variety of applications.[1,2] ZnO thin film has attracted interest as a window material for solar cells, since it is a low-cost alternative to Sn-doped In_2O_3.[1,3] Low-resistive zinc oxide thin films have been achieved by doping with different group III elements, like aluminium, boron, indium, and gallium, or with group VII elements, like fluorine.[4,5] The many deposition techniques that have been employed to deposit these ZnO thin films include sputtering,[3,6] sol–gel,[7–9] pulsed laser deposition,[10] and spray pyrolysis.[2,4,5,11]

Low-resistive ZnO films are obtained either by post-deposition heat treatment in a vacuum or hydrogen atmosphere or by adding donor impurities, such as aluminium[2] or indium.[12] In this respect, indium has been tested as a successful doping

(Received August 6, 2014; accepted November 17, 2014; published online December 4, 2014)

element amongst group III elements, because it has been reported that chemically sprayed ZnO:In films with the lowest resistivity have been achieved without a post-annealing process.[13] Despite this fact, Al doping is still of interest, because of its low cost and non-toxicity, which is in contrast to the case of expensive, toxic In compounds. Detailed work is necessary prior to reaching deposition conditions in order to enable Al doping to present a competitive TCO application, as was the case for fluorine-doped ZnO films, based on a chemical spray pyrolysis technique, or simultaneous F plus Al-doping in ZnO films, deposited by using a sol–gel technique.[9]

In an ultrasonic spray pyrolysis (USP) system, an alcoholic solution containing the precursor salts is nebulized by an ultrasonic actuator, and is then transported onto a heated substrate. The advantage of using USP over conventional pneumatic spraying is that the smaller droplets and the narrowing in the corresponding size distribution allows for better control of the spray flux with a soft carrier gas flow. This can achieve the deposition of very thin layers with homogeneous thickness, and a significant reduction of consumption of the reactants.[11,14] Lee et al. reported a resistivity of 1.71×10^{-2} Ω cm for annealed Al-doped ZnO (AZO) thin films obtained via USP, with $AlCl_3$ as a precursor.[2] In our case, the electrical properties of the films, as reported in our previous publication,[15] showed a resistivity of 1×10^{-3} Ω cm for the as-deposited AZO film with 3 at.% aluminium doping (aluminiumacetylacetonate as precursor) at 475°C using USP.

Following our previous work,[15–17] in this study we investigate the effects of aluminium doping on the structural properties of AZO films. We also report the electrical and optical properties of the un-doped ZnO, as well as the double-layered (AZO/ZnO) films deposited by using a low-cost non-vacuum USP technique. In addition, we demonstrate that post-annealing treatment of the AZO/ZnO layer in vacuum improves both the optical and electrical properties. These TCOs with optimum parameters [low resistivity of the order of 10^{-4} Ω cm, and high transmittance (≈90%)] are potential candidates for fabrication of low-cost $Cu(In_{1-x}Ga_x)Se_2$-based thin film solar cells,[17] which is the focus of the work being undertaken in our laboratory.

EXPERIMENTAL

Transparent conducting AZO thin films were prepared via USP[18] (vertical configuration type), as detailed in our previous publication.[15] A 0.2-M starting solution was prepared from zinc acetate di-hydrate [$Zn(CH_3COO)_2{\cdot}2H_2O$], dissolved in a mix of methanol and acetic acid. Aluminiumacetylacetonate ($C_{15}H_{21}AlO_6$), previously diluted in a mixture of de-ionized water and acetic acid at 0.2 M, was added in order to dope the initial Zn solution. The Al/Zn atomic ratio was taken as a reference for doping quantification. In this case, the variation in the doping concentration was set to 2 at.%, 3 at.%, and 4 at.%. The solution was sprayed onto previously cleaned soda lime glass substrates, and the droplets of the solution produced by the ultrasonic generator were carried to the substrate using nitrogen gas, at an adjusted flow rate of 1.2 mL/min. The films were deposited in air at a temperature of 475°C for 10 min. Un-doped ZnO was deposited onto the glass substrate, as well as onto AZO (3 at.% Al/Zn), using USP at 400°C for 10 min and 3 min, respectively. The post-annealing treatment was performed on the bilayer (AZO/ZnO), at 350°C in vacuum for 20 min.

Structural analyses of the films were measured according to observation through a PANalytical Xpert X-Ray Diffractometer, with $CuK_{\alpha 1}$ (λ = 1.5406 Å) and $CuK_{\alpha 2}$ (λ = 1.5444 Å) lines in the θ–2θ mode. X-ray diffraction (XRD) patterns were recorded in the scanning range of 20–80°, with a scan step of 0.04923°. Crystallite sizes (D) were calculated using Scherrer's formula,

$$D = \frac{0.94\lambda}{\beta \cos\theta}, \tag{1}$$

where β is the full width at half maximum (FWHM) of the reflected peak at the Bragg angle, θ.

The strain (ε) was calculated using the relationship,

$$\beta = \frac{\lambda}{(D\cos\theta)} - \varepsilon \tan\theta. \tag{2}$$

The dislocation density (δ) is defined as the length of the dislocation lines per unit volume of the crystal, and can be evaluated from Eq. 3:

$$\delta = \frac{1}{D^2}. \tag{3}$$

The surface morphology of the films was examined using a Carl Zeiss AURIGA field emission scanning electron microscope (FESEM), at an operating voltage of 10 kV. Cross-sectional FESEM images were taken, and the thicknesses of the samples were measured from them. The compositions of all the deposited films were determined using a Bruker energy dispersive analysis, with an x-ray (EDAX) system attached to a secondary electron microscope, set to an accelerating voltage of 10 kV. Secondary ion mass spectroscopy (SIMS) was carried out, using CAMECA-IMS6F equipment. High-resolution transmission electron microscopy (HRTEM) images were taken, using the JEOL JSM-2010F set-up. The transmittance spectra were recorded using a SHIMADZU UV–Vis double beam spectrophotometer, at a wavelength range of 300 nm to 1100 nm. Hall measurements were carried out by using the Van der Pauw method, via

Walker scientific HV-4H equipment at room temperature.

RESULTS AND DISCUSSION

Properties of AZO Thin Films

Figure 1a shows the structural evolution of the AZO thin films deposited at 475°C for different Al/Zn ratios in solution, namely from 0 (un-doped zinc oxide) to 4 at.%. The positions of the peaks match those of polycrystalline zinc oxide with a hexagonal wurtzite structure (JCPDS data, 36-1451). A peak associated with the (101) plane is found for AZO thin films, and no diffraction peaks of Al_2O_3 or other impurities were observed.[19] However, the intensity of the (002) peak decreased as the doping concentration increased, and this observation was confirmed by calculating the texture coefficient (T_c), as Fig. 1b shows. A (0 0 2) preferential crystalline orientation along the *c*-axis perpendicular to the substrate surface is commonly observed in ZnO thin films, regardless of the film deposition technique used.[20] This particular orientation follows the evolutionary grain selection model proposed by Knuyt et al.,[21] and usually correlates with the energies gained by the incident species on the substrate under appropriate experimental conditions. The wurtzite structure consists of triangularly arranged alternating diatomic close-packed (0001) planes, for example, Zn and O pairs. Thus, the stacking sequence of the (0001) plane is *AaBbAaBb*… in the ⟨0001⟩ direction.[22] However, non-optimal experimental conditions, defects, and other chemical impurities may hinder the (0 0 2)-oriented growth.[15]

It is clear from Table I that the crystallite size of the ZnO micro-crystallites increased, and the strain and dislocation density decreased, as the Al/Zn ratio in solution increased up to 3 at.%. Further increase in the doping concentration deteriorates the crystallinity of the films, possibly due to the formation of stress induced by the difference in the ion sizes between Zn and Al (r^{2+}_{Zn} = 0.074 nm and r^{3+}_{Al} = 0.054 nm), and the segregation of Al in the grain boundaries for high doping concentrations.[2,15] Extra Al atoms might not occupy their appropriate sites inside the ZnO crystallites, because the solubility limits of Al into ZnO lattice have been overcome. This Al excess may occupy interstitial positions, and would then deform the micro-crystalline structure.[23] Figure 2a–d shows FESEM images of AZO thin films deposited at 475°C with Al/Zn ratios of 0 at.%, 2 at.%, 3 at.%, and 4 at.%, respectively. These images reveal that the surface morphology of the films is strongly dependent on the concentration of the aluminium. For the un-doped films, broken hexagons can be observed, in contrast with what was found in films with pneumatic spray pyrolysis, where well-defined hexagons form.[24–26] As can be seen from the micrographs, the grain size varied as the doping concentration increased, due to differences in the ionic radii of zinc and aluminium.[7,24] At higher Al/Zn concentrations, the development of

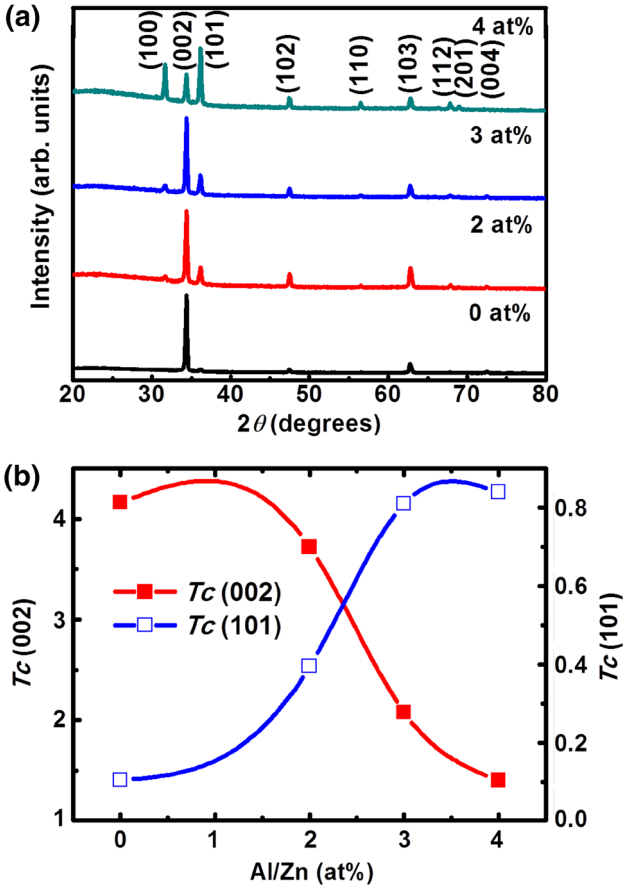

Fig. 1. (a) XRD patterns of the AZO thin films, and (b) texture coefficients (T_c) of (002) and (101) peaks, for different Al/Zn ratios deposited at 475°C.

agglomerates from the small spiral grains (Fig. 2b) gives rise to elongated secondary grains, as observed in Fig. 2c. After reaching the critical aluminium concentration, Al tends to segregate at the grain boundaries, hindering the development of longer grains, as Fig. 2d shows.[14,27]

Table II gives details of the chemical composition obtained via EDAX for 0 at.%, 2 at.%, 3 at.%, and 4 at.% AZO thin films. The average atomic percentages of zinc and oxygen were 57.49 and 41.89, respectively, which indicates that the films were oxygen-deficient in nature. The oxygen deficiencies are known to give rise to electrical conductivity in TCOs.[28] It is clear from Table II that the aluminium concentration in the films is less than that of the starting solution. We noticed the same trend in all the films deposited by USP at 475°C, and SIMS also verified this (Fig. 3). As a consequence of the re-evaporation of the components during the deposition process, the concentration in the chemical composition of the films is lower, as compared to the concentration of precursors in the starting solution. It is worth noting that Al quantification is also a problem when performed using conventional techniques, like measuring x-rays emitted by transitions

Table I. Structural parameters of AZO thin films with different Al/Zn ratios in the precursor solution deposited at 475°C

Al/Zn ratio (at.%)	Crystallite size, D (nm)	Strain, $\varepsilon \times 10^{-4}$ (lines^{-2}m^{-4})	Dislocation density, $\delta \times 10^{15}$ (lines/m^{-2})
0	23.35	14.42	1.83
2	31.90	10.57	0.97
3	34.50	9.79	0.83
4	33.20	10.18	0.96

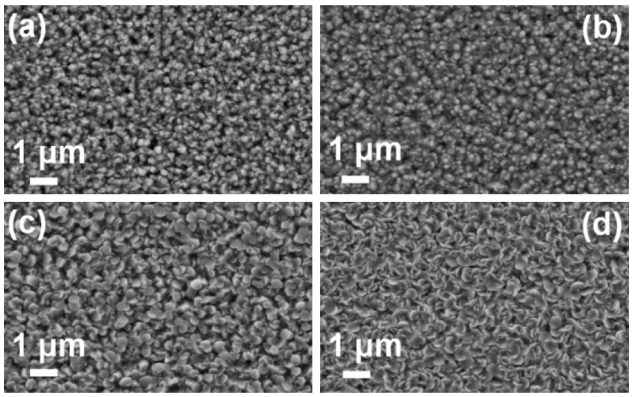

Fig. 2. FESEM images of the AZO thin films deposited at 475°C with different Al/Zn ratios in precursor solution: (a) 0 at.%, (b) 2 at.%, (c) 3 at.%, and (d) 4 at.%.

from K_α and K_β levels. Hence, for more precise determination, the films were subjected to SIMS analyses, to reveal both the stoichiometry of the films and the percentage of the incorporation of Al into the AZO thin films. Figure 3 shows the atomic concentration as a function of the time of exposure for the film deposited with a ratio of Al/Zn = 3 at.% in solution. A similar analysis was made for films deposited with Al/Zn = 2 at.% and 4 at.%. As a result, the films deposited with a doping of 2 at.%, 3 at.%, and 4 at.% showed ppm values of Al of 2.4×10^3, 4.3×10^3, and 4.6×10^3, respectively, which correspond to the percent values of Al/Zn = 0.24, 0.43, and 0.46, respectively. This analysis shows that AZO films exhibited a homogenous composition, but the ratio of Zn/O was, in general, greater than 1. This suggests the non-stoichiometric structural properties of ZnO, which are in agreement with other reports.[29] It should be noted that the precise location of Al, whether it is in Zn sites or passivating electric active sites in the grain boundaries, is still a matter of controversy.[9]

Figure 4a shows an HRTEM image of a typical AZO thin film deposited with an Al/Zn ratio of 3 at.% in solution. The inset shows a fast Fourier transform (FFT), with reflections corresponding to (1 0 0), (1 0 −2), (−1 0 −2), and (200) crystalline planes, with d spacings of 0.28 nm, 0.19 nm, 0.17 nm, and 0.14 nm, respectively, which is consistent with

Table II. EDAX analyses of AZO thin films with different Al/Zn ratios in the precursor solution deposited at 475°C

Al/Zn ratio (at.%)	Zn (at.%)	O (at.%)	Al (at.%)
0	57.73	42.27	–
2	57.13	42.55	0.33
3	58.04	41.44	0.52
4	56.89	42.48	0.63

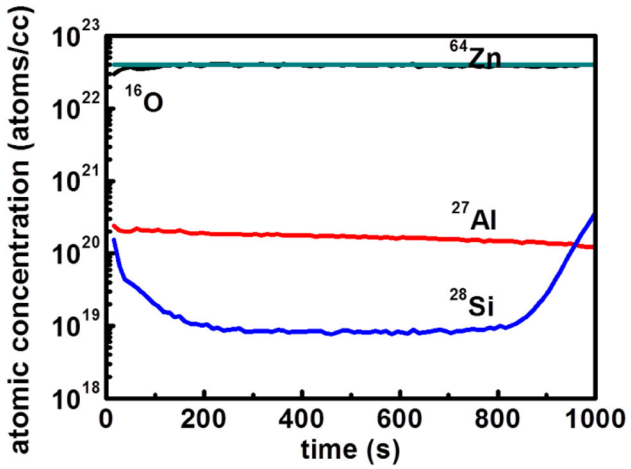

Fig. 3. SIMS analyses of the AZO thin film with 3 at.% Al/Zn ratio deposited at 475°C.

the XRD (JCPDS, 36-1451) observations that confirmed the hexagonal wurtzite structure. The absence of the (002) ring in the FFT of the AZO film indicates that c-axis growth is preferentially oriented parallel to the film surface.[30] Local formation of Al_2O_3 was not detected in the FFT, possibly as a result of the low content of Al incorporated into the ZnO lattice, and the fact that Al replaces Zn. Also, the HRTEM image of the AZO thin films was simulated using the Simula-TEM software for hexagonal structure, matched with the experimental results, as shown in the inset of the inverse FFT (IFFT) given in Fig. 4b. As shown in the inset of Fig. 4c, the simulated (0 1 0) plane matched that of

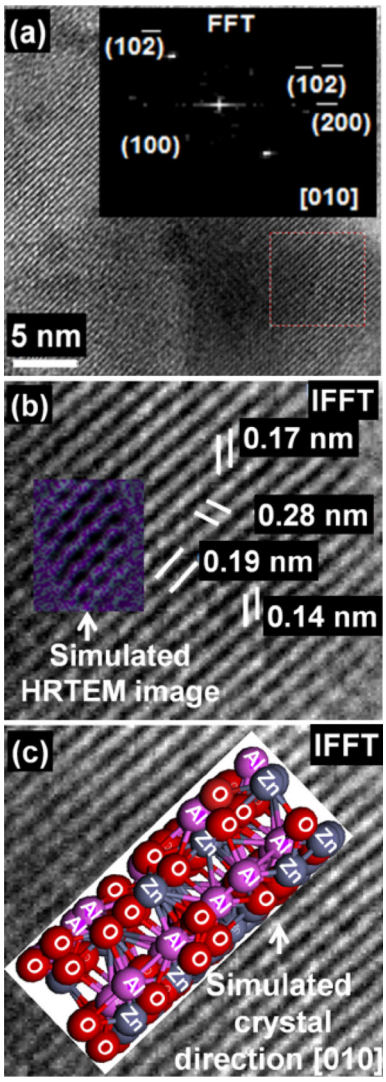

Fig. 4. HRTEM analyses of the AZO thin film with 3 at.% Al/Zn ratio deposited at 475°C. The inset in (a) shows an FFT of the selected area in the image, (b) an inverse FFT with calculated *d*-spacing, and the inset depicts the simulated HRTEM image, while the inset in (c) shows the simulated crystal direction.

the experimental result, confirming that the orientation corresponded to this particular plane.[31] The simulations proved that the AZO films grown using USP at 475°C were polycrystalline hexagonal in nature.

Properties of Un-doped ZnO on a Glass Substrate

Figure 5a shows the transmittance spectra in the range of 300–1000 nm for the ZnO thin films deposited at a substrate temperature of 400°C. The deposited films exhibited a visible light transmittance of about 80%. The inset in Fig. 5 shows a plot of $(\alpha h\nu)^2$ versus $h\nu$ for the film deposited at a substrate temperature of 400°C. ZnO showed an absorption edge at 375 nm, corresponding to a band gap of 3.22 eV. This film showed a resistivity of

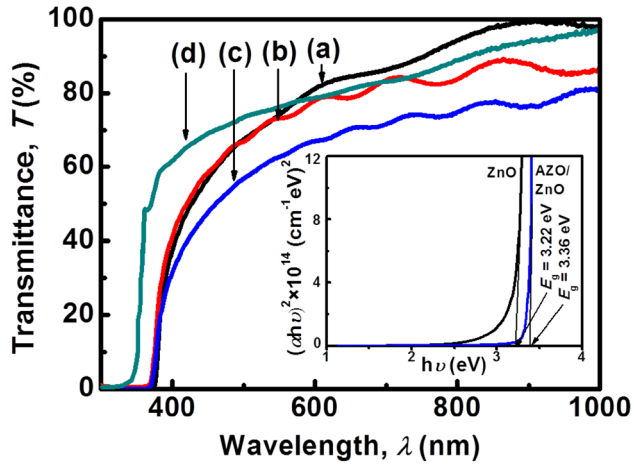

Fig. 5. Transmittance spectra of the (a) un-doped ZnO, (b) AZO, (c) AZO/ZnO bi-layer, and (d) annealed AZO/ZnO bi-layer thin films deposited at 400°C, 475°C, 475°C/400°C and annealed at 350°C, respectively. The inset depicts the $h\nu$ versus $(\alpha h\nu)^2$ graph for the un-doped ZnO and AZO/ZnO bi-layer.

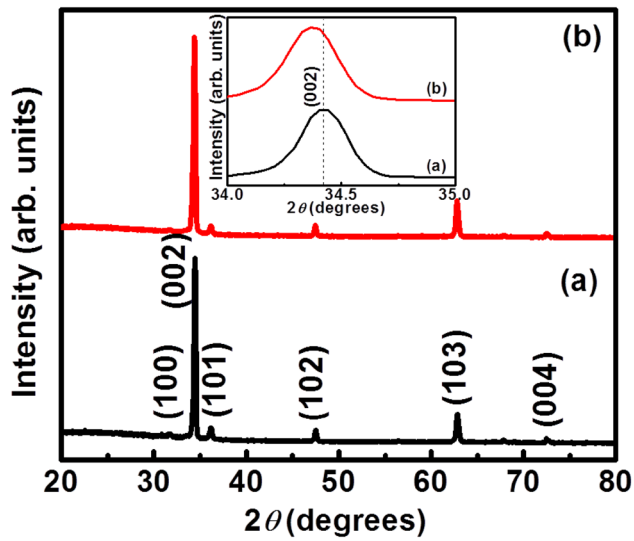

Fig. 6. XRD patterns of (a) AZO, and (b) AZO/ZnO layers deposited on glass at 475°C and 475°C/400°C, respectively; the inset shows the selected angle diffraction patterns of (a) and (b).

43.69 Ω cm, mobility of 3.4 cm^2/V s, and a carrier concentration of 4.81×10^{16} cm^{-3}. Low carrier concentration and conductivity indicate the intrinsic nature of the ZnO thin film without any additional doping.[13] Normally, un-doped ZnO with a wurtzite structure becomes an *n*-type semiconductor as a result of the presence of intrinsic or extrinsic defects, which are generally attributed to native defects, such as Zn on an O antisite (Zn_O), Zn interstitial (Zn_I), and an O vacancy (V_O).[22]

Properties of AZO/ZnO Bilayer

Based on the structural, morphological, electrical, and optical properties of AZO thin films reported

here and in previous work,[15] we proceeded with further studies of the 3 at.% Al/Zn film deposited at 475°C. Figure 6a and b shows the XRD patterns of the ZnO film deposited on bare glass and onto AZO substrate, respectively. These films crystallized in a hexagonal wurtzite structure, with a preferential orientation along the (0 0 2) direction. These results are consistent with the JCPDS data card no. 36-1451. As the inset of Fig. 6 shows, the position of the (002) peak shifted from 34.40° to 34.36°, as a result of the deposition of un-doped ZnO, indicating stress in the film. This stress is related to defects in the films, and the compressive stress may be a result of the zinc interstitials. However, the tensile stress is likely to be a result of the oxygen vacancies that exist in the ZnO thin film crystallites.[32]

Figure 7a shows FESEM micrographs of the ZnO thin film on the AZO substrate. As this image reveals, the film grew vertically onto the surface with a broken hexagonal columnar structure. Nevertheless, the film deposited on the AZO-coated glass had a dense morphology with small grains. Figure 7b presents the cross-section of ZnO film deposited on the AZO substrate, where the film seems to be homogeneous, with a thickness of around 300 nm. The XRD characterization suggests that the intense (002) peak of the ZnO films is related to the density of the films.[32]

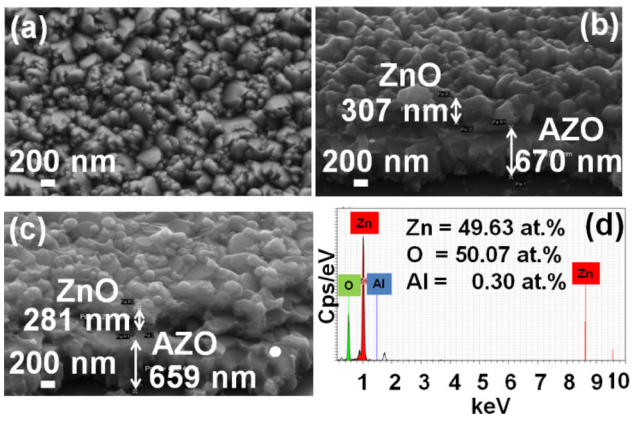

Fig. 7. (a) Surface morphology, (b) cross-sectional view of un-doped ZnO on AZO deposited at 400°C before annealing, (c) after annealing at 350°C in vacuum, and (d) point analysis of the AZO layer shown in (c).

Figure 5b and c shows the transmittance spectra of AZO with and without the ZnO layer, respectively, with a wavelength range of 300–1000 nm. The AZO films with and without the ZnO layer yielded transmittances of 70% and 80%, respectively. The increase in the transmittance is associated with a decrease in film thickness. The interference fringes in the transmission spectra of the ZnO deposited on AZO-coated glass confirm that the film thickness is uniform. The optical bandgap of the AZO/ZnO bi-layer is 3.36 eV, as obtained from the inset of Fig. 5. Table III shows the electrical parameters of the AZO thin film, and of the AZO/ZnO bilayer. Upon deposition of the un-doped ZnO layer on the AZO layer, both the carrier concentration and the Hall mobility increased, and the film resistivity was lower than that of a single AZO film. Earlier studies also demonstrated that bilayer film of AZO/ZnO prepared via sputtering had lower resistivity than that of single-layered AZO film.[33]

Post-annealing Treatment of AZO/ZnO Bi-layer

In order to improve the optical transmittance and conductivity of the AZO/ZnO bi-layer, post-annealing was performed at 350°C in vacuum for 20 min. Figure 7c shows across-sectional image of the annealed AZO/ZnO bi-layer that presented improved crystallinity relative to the as-deposited film given in Fig. 7b. Figure 7d shows the point analysis on the AZO layer that was carried out to confirm the stability of the layer through un-doped ZnO deposition and heat treatment. The most obvious observation with respect to the annealed films is the improvement in the transmittance due to the enhanced crystallinity, and the decrease in the carrier scattering, as Fig. 5d shows. Table III indicates another observation that is worth noting for the heat-treated samples: the decrease in resistivity (3.6×10^{-3}–2.6×10^{-3} Ω cm), and increase in mobility (3.2–13.8 cm^2/V s).

The following conclusions can be drawn with respect to the annealed films:

(i) in the as-deposited films, a large density of extrinsic traps is present at the grain boundaries due to oxygen chemisorption; this in turn depletes the grain and results in a barrier-to-carrier conduction at the grain boundaries;

Table III. Electrical parameters of AZO, AZO/ZnO, and annealed AZO/ZnO bi-layers deposited on glass at 475°C, 475°C/400°C and annealed at 350°C in vacuum, respectively

Sample Identification	Resistivity, ρ (Ω cm)	Mobility, μ (cm^2/V s)	Carrier concentration, n (cm^{-3})
AZO	5.8×10^{-3}	2.9	3.65×10^{20}
AZO/ZnO	3.6×10^{-3}	3.2	5.51×10^{20}
Annealed AZO/ZnO	2.6×10^{-3}	13.8	1.75×10^{20}

(ii) annealing in vacuum or in a reducing ambient desorbs oxygen from the grain boundaries, as well as from the bulk, thereby reducing the potential barriers at the grain boundaries and increasing the effective carrier concentration;
(iii) re-annealing in an oxygen ambient causes the chemisorption of oxygen once more, reversing this process.[34]

CONCLUSIONS

Uniform, adherent AZO thin films were deposited on soda lime glass substrates by using a low-cost, non-vacuum, ultrasonic spray technique, with the objective of fabricating all spray CIGS-based photovoltaic devices. XRD studies revealed a hexagonal wurtzite structure for the AZO thin films. The morphology of the films changes according to the Al content in the ZnO lattice. Composition analysis measured the percentage of incorporation of Al into the AZO thin films, and local analysis of the grains showed the atomic arrangements of the films, confirming the wurtizte structure, and absence of Al_2O_3 clusters. Simulation of the corresponding crystal plane that matched the HRTEM pattern confirmed the orientation of the film. The electrical properties of the un-doped ZnO showed the intrinsic nature of the film. The transmittance of the AZO/ZnO bi-layer was lower than that of the AZO layer; whereas it increased after annealing in vacuum. The resistivity of the as-deposited and annealed AZO/ZnO bi-layer was less than that of the as-deposited single and bi-layers. Thus, we demonstrated an improvement in the optical and electrical properties of the AZO and AZO/ZnO layers deposited via USP.

ACKNOWLEDGEMENTS

The authors wish to thank Dr. Jaime Vega Perez, Miguel Avendaño, and Roberto Hernández for providing technical assistance. Our special thanks to Dr. A. Maldonado for providing the USP facilities, and for useful discussions. We extend our thanks to Dr. Yuriy Kudriavtsev for the SIMS measurements. B.J. Babu is grateful to CONACyT for receiving a scholarship to pursue a Doctoral program in Mexico. The authors also wish to thank ICyTDF for the financial support provided through project 326/11.This work is also supported by a Human Resources Development Program Grant (No. 20124010203280) of the Korea Institute of Energy Technology Evaluation and Planning (KETEP), funded by the Ministry of Trade, Industry and Energy of the Korean government. One of the authors (S.V.) is grateful for the support from MSIP (Ministry of Science, ICT & Future Planning), (141S-6-3-0641), South Korea.

REFERENCES

1. H. Kashani, *J. Elect. Mater.* 27, 876 (1998).
2. J.H. Lee and B.O. Park, *Mater. Sci. Eng. B* 106, 242 (2004).
3. J. Yoo, J. Lee, S. Kim, K. Yoon, I. Jun Park, S.K. Dhungel, B. Karunagaran, D. Mangalaraj, and J. Yi, *Thin Solid Films* 480/481, 213 (2005).
4. B. Joseph, P.K. Manoj, and V.K. Vaidyan, *Ceram. Int.* 32, 487 (2006).
5. R.R. Biswal, S. Velumani, B.J. Babu, A. Maldonado, S. Tirado-Guerra, L. Castañeda, and M. de la L. Olvera, *Mater. Sci. Eng. B* 174, 46 (2010).
6. G. Fang, D. Li, and B. Yao, *Vacuum* 68, 363 (2003).
7. H. Zhou, D. Yi, Z. Yu, L. Xiao, and J. Li, *Thin Solid Films* 515, 6909 (2007).
8. K.J. Chen, T.H. Fang, F.Y. Hung, L.W. Ji, S.J. Chang, S.J. Young, and Y.J. Hsiao, *Appl. Surf. Sci.* 254, 5791 (2008).
9. D.C. Altamirano-Juárez, G. Torres-Delgado, S. Jiménez-Sandoval, O. Jiménez-Sandoval, and R. Castanedo-Pérez, *Sol. Energy Mater. Sol. Cells* 82, 35 (2004).
10. S. Venkatachalam, Y. Iida, and Y. Kanno, *Superlattices Microstruct.* 44, 127 (2008).
11. Y. Lee, H. Kim, and Y. Roh, *Jpn. J. Appl. Phys.* 40, 2423 (2001).
12. J.H. Lee, S.Y. Lee, and B.O. Park, *Mater. Sci. Eng. B* 127, 267 (2006).
13. C.E. Benouis, A. Sanchez-Juarez, and M.S. Aida, *J. Appl. Sci.* 7, 220 (2007).
14. S. Oktik, *Prog. Crystal Growth and Charact.* 17, 171 (1988).
15. B.J. Babu, A. Maldonado, S. Velumani, and R. Asomoza, *Mater. Sci. Eng. B* 174, 31 (2010).
16. B.J. Babu, A. Maldonado, and S. Velumani, *6th International Conference on Electrical Engineering, Computing Science and Automatic Control* (2009). doi:10.1109/ICEEE.2009.5393563.
17. B.J. Babu, S. Velumani, and R. Asomoza, *Photovoltaic Specialists Conference* (2011). doi:10.1109/PVSC.2011.6186181.
18. X. Zhang, H. Fan, J. Sun, and Y. Zhao, *Thin Solid Films* 515, 8789 (2007).
19. M.A. Kaid and A. Ashour, *Appl. Surf. Sci.* 253, 3029 (2007).
20. L. Hadjeris, L. Herissi, M.B. Assouar, T. Easwarakhanthan, J. Bougdira, N. Attaf, and M.S. Aida, *Semiconduct. Sci. Technol.* 24, 035006 (2009).
21. G. Knuyt, C. Quaeyhaegens, J.D. Haen, and L.M. Stals, *Phys. Status Solidi B* 195, 179 (1996). doi:10.1002/pssb.2221950121.
22. U. Ozgur, Y.I. Alivov, C. Liu, A. Teke, M.A. Reshchikov, S. Dogan, V. Avrutin, S.J. Cho, and H. Morkoc, *J. Appl. Phys.* 98, 041301 (2005).
23. R. Romero, D. Leinen, E.A. Dalchiele, J.R. Ramos-Barrado, and F. Martin, *Thin Solid Films* 515, 1942 (2006).
24. Y. Lee, H. Kim, and Y. Roh, *Jpn. J. Appl. Phys.* 40, 2423 (2001).
25. M. Krunks, T. Dedova, and I. OjaAcik, *Thin Solid Films* 515, 1157 (2006).
26. M. de la L. Olvera, A. Maldonado, Y. Matsumoto, R. Asomoza, M.A. Melendez-Lira, and D.R. Acosta, *J. Vac. Sci. Technol.* A19, 2097 (2001).
27. H. Gomez-Pozos, A. Maldonado, and M. de la L. Olvera, *Mater. Lett.* 61, 1460 (2007).
28. T. Prasada Rao and M.C. Santhosh Kumar, *Appl. Surf. Sci.* 255, 4579 (2009).
29. Y.K. Moon, S.H. Kim, and J.W. Park, *J. Mater. Sci. Mater. Electron.* 17, 973 (2006).
30. A.F. Aktaruzzaman, G.L. Sharma, and L.K. Malhotra, *Thin Solid Films* 198, 67 (1991).
31. B. Vidhya, S. Velumani, J.A. Arenas-Alatorre, A. Morales-Acevedo, R. Asomoza, and J.A. Chavez-Carvayar, *Mater. Sci. Eng. B* 174, 216 (2010).
32. M. Mekhnache, A. Drici, L. SaadHamideche, H. Benzarouk, A. Amara, L. Cattin, J.C. Bernede, and M. Guerioune, *Superlattices Microstruct.* 49, 510 (2011).
33. J.H. Shi, S.M. Huang, J.B. Chu, H.B. Zhu, Z.A. Wang, X.D. Li, D.W. Zhang, Z. Sun, W.J. Cheng, F.Q. Huang, and X.J. Yin, *J. Mater. Sci. Mater. Electron.* 21, 1005 (2010).
34. E. Shanthi, A. Banerjee, V. Dutta, and K.L. Chopra, *Thin Solid Films* 71, 237 (1980).